Quantifying the Reproducibility of Multi-Band High Speed Wireless Channel Measurements

Faruk Pasic*, Markus Hofer†, Danilo Radovic*, Herbert Groll*, Sebastian Caban*,
Thomas Zemen† and Christoph F. Mecklenbräuker*

*Institute of Telecommunications, TU Wien, Vienna, Austria

†AIT Austrian Institute of Technology, Vienna, Austria

faruk.pasic@tuwien.ac.at

***Abstract*—Future vehicular communication systems will extend deployed frequency bands from sub-6 GHz to millimeter wave (mmWave). To investigate different propagation effects between sub-6 GHz and mmWave bands in high-mobility scenarios, we proposed a suitable testbed setup to compare these two bands in a fair manner. Experiments conducted using the proposed testbed provide realistic results, but they are only usable if they can be faithfully reproduced. To quantify the reproducibility of the proposed testbed, we perform channel measurements at center frequencies of 2.55 GHz and 25.5 GHz at a velocity of 50 km/h. We investigate the influence of antenna pattern, time between measurements, signal-to-interference-and-noise ratio (SINR) and signal bandwidth on the reproducibility in terms of the channel correlation.**

***Index Terms*—mmWave, sub-6 GHz, 5G, high-mobility, vehicular communications, testbed, channel measurements, correlation, reproducibility.**

I. Introduction

Wireless communication and sensing technologies for vehicles are expected to support a wide variety of safety-related applications in vehicular networks, such as object detection, risk identification and car platooning [1], [2]. These applications require high data transmission rates for information exchange between vehicles, which conventional sub-6 GHz bands cannot support due to the spectrum shortage. On the other hand, millimeter wave (mmWave) bands (10 GHz – 300 GHz) provide rich spectrum resources, hence allowing for significantly higher data rates [3]. For this reason, developing mmWave communication systems for vehicle-to-everything (V2X) scenarios is attracting more attention.

Propagation at sub-6 GHz bands has been well investigated in realistic high-mobility environments [4]–[13]. In addition to sub-6 GHz bands, time-variant radio channels have also been investigated at mmWave bands through real-world measurements [14]–[20]. To learn how propagation and scattering effects change from sub-6 GHz to mmWave bands, comparative measurements over different bands have been conducted [21]–[25]. In [26], we proposed a testbed and methodology to enable a fair comparison between sub-6 GHz and mmWave bands in a controlled high-mobility environment. Our proposed testbed setup allows wireless channel measurements from the same transmitter and receiver position, with the same transmitter velocity, but at different frequencies, which is hardly possible by conducting real-world drive-by measurements.

Our proposed testbed operates at a center frequency of 2.55 GHz and 25.5 GHz, which correspond to fifth generation (5G) new radio (NR) frequency bands n7 and n258, respectively [27]. Choosing a frequency within 5G NR frequency band implies that undesired interference from other transmitters may inherently influence every single measurement, as the testbed does not include an anechoic environment to guarantee radio frequency (RF) isolation. In addition, equipment malfunction could degrade the timing and/or frequency synchronization of our testbed. All these undesired factors could impact reproducibility[1], which is the main attribute of our proposed testbed.

Contribution: We quantify the reproducibility of wireless channel measurements performed at 50 km/h at two different frequency bands. We use a static receiver and we mount the moving transmitter on the top of a rotating arm. This setup allows us to measure wireless channels at sub-6 GHz (2.55 GHz) and mmWave (25.5 GHz) bands in the *same* high-mobility environment. We investigate the impact of different receive antenna radiation patterns on the reproducibility of the measurements. Specifically, we compare the measurements in terms of channel correlation against time, signal-to-interference-and-noise ratio (SINR), position over measured trace and signal bandwidth to objectively quantify to what extent we have reproduced the experiment.

The rest of the paper is organized as follows. Section II describes our testbed for sub-6 GHz and mmWave channel measurements. The measurement campaign to capture the reproducibility of experimental results is described in Section III. In Section IV, we quantify the reproducibility and discuss the results in terms of channel correlation. Finally, Section V concludes the paper.

Notation: Matrices are denoted by bold uppercase letters such as $\mathbf{H}$ and vectors by bold lowercase letters $\mathbf{h}$. The entries of matrices and vectors are accessed by subscripts, e.g. $\mathbf{H}_t$. We use the superscript $(\cdot)^{\mathrm{H}}$ for conjugate transposition, $\|\cdot\|_F$ denotes the Frobenius norm and $\|\cdot\|_2$ denotes the Euclidean norm. Also, we denote the absolute value by $|\cdot|$ and the trace of a matrix by $\mathrm{tr}\,(\cdot)$.

[1]Reproducibility is the closeness of agreement between independent results obtained with the same method on identical test material but under different conditions (different operators, different apparatus, different laboratories and/or after different intervals of time) [28].

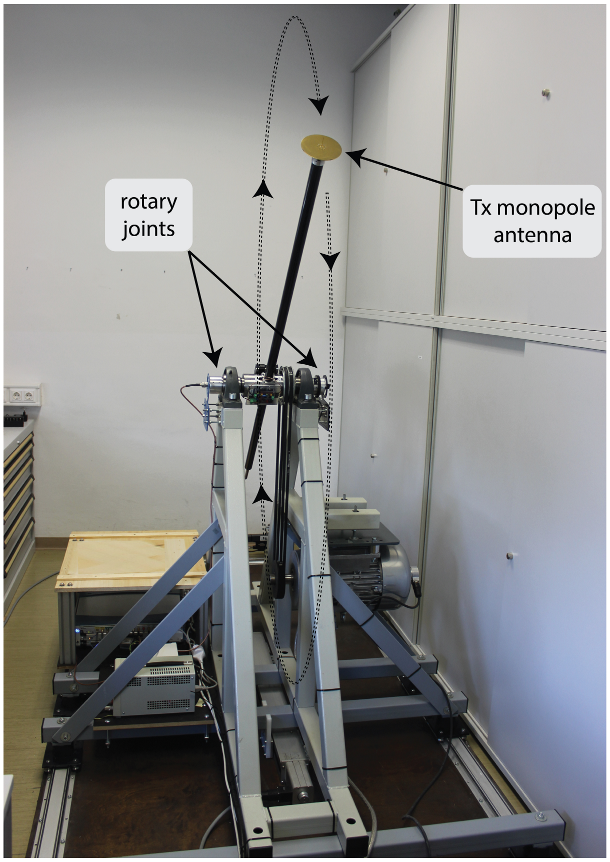

Fig. 1. The rotary unit rotates a vertical monopole transmit antenna at the velocity of 50 km/h. A measurement is triggered at each revolution at the same position.

II. Testbed Design

Our testbed setup is described in [29] and consists of a moving transmitter and a static receiver. The moving transmitter is based on a rotary unit described in [30]. The rotary unit (see Fig. 1) rotates an antenna placed at the end of a 1 m long arm around a central axis at a constant but adjustable velocity of up to 400 km/h. This rotary unit is equipped with a trigger unit, which generates a trigger pulse at a precisely defined angle to start the measurement once per revolution. The trigger pulse is fed to the transmitter and receiver via cables to ensure precise time synchronization. To provide precise frequency synchronization, the transmitter and receiver are interconnected with a 10 MHz reference. There are also rotary joints at each end of the central axis to feed transmit signals from a signal source to the rotating antenna. The testbed setup operates in sub-6 GHz and mmWave bands. In the sub-6 GHz case, the RF signal is directly fed to the transmit antenna. In the mmWave case, we use a mmWave transmitter [26] mounted at the end of the rotary arm to generate the RF signal.

III. Measurement Campaign

Using the testbed setup from Section II, we perform wireless channel measurements in an indoor environment, as shown

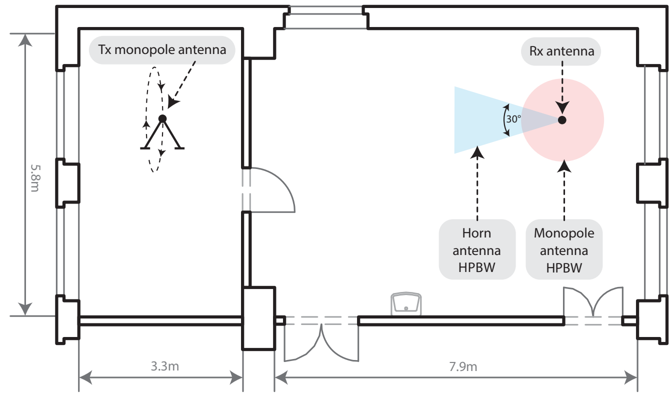

Fig. 2. Measured indoor laboratory environment. The moving transmit antenna and the static receive antenna are located in neighboring rooms.

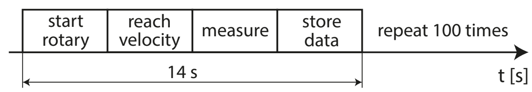

Fig. 3. The time required for a single measurement run is 14 seconds. We execute 100 measurement runs consecutively for different receive antennas at two different frequency bands.

in Fig. 2. The transmit antenna is mounted on the rotary unit and is moving on a circular arc segment (from $-40°$ to $40°$) with the constant velocity of 50 km/h. Note that the angular position of $0°$ corresponds to the direction normal to the ceiling. A receive antenna is placed in a neighboring room about 7.5 m apart from the transmit antenna and is static on a laboratory table.

To investigate the reproducibility and degree of variability of the measurement results, we conduct $T = 100$ identical consecutive experiments (measurement runs) over time. On the transmitter side, we use a vertical monopole antenna, which rotates around the central axis. On the receiver side, we alternate between a horn antenna with 30 ° half-power beamwidth (HPBW) and a vertical monopole antenna. Specifically, we conduct 100 consecutive measurements for each of the four measurement combinations: horn or vertical monopole receive antenna and sub-6 GHz (2.55 GHz) or mmWave (25.5 GHz) center frequency. Within a single measurement run, the total time required to start the rotary unit, reach the velocity of 50 km/h, conduct the measurement and store the measurement data to hard disk is 14 seconds (see Fig. 3). To keep the fading environment static, we conduct the measurements within 3 hours with no people or moving objects within the room. Furthermore, the transmit antenna trace (arc segment) and the receive antenna position remain unchanged. The measurement parameters are provided in Tab. I.

A. Measurement Procedure

We transmit a sequence of 50 000 identical orthogonal frequency-division multiplexing (OFDM) transmit symbols designed using a Zadoff-Chu sequence [31]. At the receiver side, we divide the measurement sequence into 500 snapshots

TABLE I
MEASUREMENT PARAMETERS

Parameter	Value
Total Bandwidth	$B_{\mathrm{t}} = 100\,\mathrm{MHz}$
Number of Subcarriers	$K = 200$
number of repetitions	$T = 100$
number of snapshots	$N = 500$
symbols per snapshot	$N_{\mathrm{sym}} = 100$
subcarrier spacing	$\triangle f = 500\,\mathrm{kHz}$
transmitter velocity	$v_{\mathrm{Tx}} = 50\,\mathrm{km/h}$
symbol duration	$t_{\mathrm{s}} = 2\,\mu\mathrm{s}$
snapshot duration	$t_{\mathrm{snap}} = 200\,\mu\mathrm{s}$
transmit power	$P_{\mathrm{Tx}} = 10\,\mathrm{dBm}$
transmit antenna	5 dBi vertical monopole antenna

of 100 symbols each, assuming that the wireless channel is constant in time for the duration of one snapshot. Further, we exploit the first OFDM symbol of each snapshot as a cyclic prefix, discard it, and perform averaging of the remaining 99 symbols to improve the signal-to-noise ratio (SNR). Finally, we obtain an estimated time-variant channel transfer function (CTF) $\mathbf{H} \in \mathbb{C}^{T\times N\times K}$ via least-square estimation, where T represents the total number of measurement runs or repetitions $t \in \{1, \ldots, T\}$, N denotes the number of discrete-time snapshots $n \in \{1, \ldots, N\}$ and K represents the number of subcarriers $k \in \{-K/2, \ldots, K/2 - 1\}$.

IV. RESULTS AND DISCUSSION

For each of the measured scenarios, we firstly calculate the SINR and then quantify the reproducibility by evaluating the correlation over (a) time, (b) SINR, (c) position within the measured trace and (d) the bandwidth employed.

A. Signal to interference and noise ratio (SINR)

The SINR is obtained by setting subcarriers $\mathcal{Z} = \{-K/2, 0, K/2\}$ that are not too close to each other to zero. The SINR is then calculated by obtaining the signal plus interference plus noise power at the non-zero subcarrier positions $\mathcal{D}$ and the interference plus noise power at the $N_{\mathcal{Z}} = 3$ zero subcarrier positions $\mathcal{Z}$ as

$$\mathrm{SINR} = \frac{\overline{P}_{\mathrm{SIN}} - \overline{P}_{\mathrm{IN}}}{\overline{P}_{\mathrm{IN}}} = \frac{\overline{P}_{\mathrm{SIN}}}{\overline{P}_{\mathrm{IN}}} - 1 = \frac{\frac{1}{TN(K-N_{\mathcal{Z}})}\sum_{t=1}^{T}\sum_{n=1}^{N}\sum_{k\in D}|y_{t,n,k}|^2}{\frac{1}{TNN_{\mathcal{Z}}}\sum_{t=1}^{T}\sum_{n=1}^{N}\sum_{k\in Z}|y_{t,n,k}|^2} - 1, \quad (1)$$

where $y_{t,n,k}$ is the received symbol at measurement run t, snapshot n and subcarrier k. The obtained values of mean received signal power $\overline{P}_{\mathrm{S}} = \overline{P}_{\mathrm{SIN}} - \overline{P}_{\mathrm{IN}}$, mean interference plus noise power $\overline{P}_{\mathrm{IN}}$ and resulting SINR for different scenarios are given in Tab. II.

TABLE II
MEASURED SINR

Frequency Band	Receive Antenna	$\overline{P}_{\mathrm{S}}$ [dBm]	$\overline{P}_{\mathrm{IN}}$ [dBm]	SINR [dB]
2.55 GHz	Horn	-48.1	-64	15.9
	Monopole	-50.9	-64.1	13.2
25.5 GHz	Horn	-67.5	-71.9	4.4
	Monopole	-76.6	-80.3	3.7

As expected, the levels of received signal power $\overline{P}_{\mathrm{S}}$ for mmWave scenarios are about 19 to 25 dB lower than for corresponding sub-6 GHz scenarios due to larger path loss. Considering the same transmit power of $P_{\mathrm{Tx}} = 10\,\mathrm{dBm}$ and the same transmit antenna gain of 5 dBi, the SINR values for mmWave scenarios are lower compared to those of sub 6-GHz scenarios. The interference plus noise power levels $\overline{P}_{\mathrm{IN}}$ for mmWave scenarios are 8 to 16 dB lower compared to the corresponding sub-6 GHz scenarios.

B. Correlation against Time

To quantify the reproducibility of different scenarios, we analyze the correlation of the CTF measured at the same position (over the same measured trace) but at different times. This examines how "similar" the measured channel is between transmissions that are temporally separated by Δt. As correlation metric, we employ the correlation coefficient given by

$$r_{\Delta t} = \frac{\left|\mathrm{tr}\left(\mathbf{H}_t^{\mathrm{H}}\mathbf{H}_{t+\Delta t}\right)\right|}{\|\mathbf{H}_t\|_F\|\mathbf{H}_{t+\Delta t}\|_F}, \quad (2)$$

where $\mathbf{H}_t \in \mathbb{C}^{N\times K}$ is the CTF corresponding to the measurement run t. The correlation $r_{\Delta t}$ is plotted against the time difference Δt between two channel measurements in Fig. 4a.

In the sub-6 GHz scenarios, the smallest observed values of $r_{\Delta t}$ for both the horn and monopole antennas are approximately 0.99. On the other hand, the mmWave scenarios show a smaller temporal correlation due to the lower SINR values. In particular, for the mmWave horn and monopole antennas, the smallest values of $r_{\Delta t}$ are 0.95 and 0.8, respectively. Although the correlation against time decreases with the measured SINR level, the system can be considered as stable over 100 repetitions or a duration of about 20 minutes.

C. Correlation against SINR

Further, we investigate how different SINR levels affect reproducibility. For each scenario mentioned above, we add complex Gaussian noise of variable power to the received signal. In this way, we obtain the estimated time-variant CTF for different SINR values, denoted as $\mathbf{H}_{t,\mathrm{SINR}}$. Then, we calculate the correlation coefficient for each SINR level and average it over T repetitions

$$\overline{r}_{\mathrm{SINR}} = \frac{1}{T}\sum_{\Delta t=0}^{T-1}\frac{\left|\mathrm{tr}\left(\mathbf{H}_{t,\mathrm{SINR}}^{\mathrm{H}}\mathbf{H}_{t+\Delta t,\mathrm{SINR}}\right)\right|}{\|\mathbf{H}_{t,\mathrm{SINR}}\|_F\|\mathbf{H}_{t+\Delta t,\mathrm{SINR}}\|_F}. \quad (3)$$

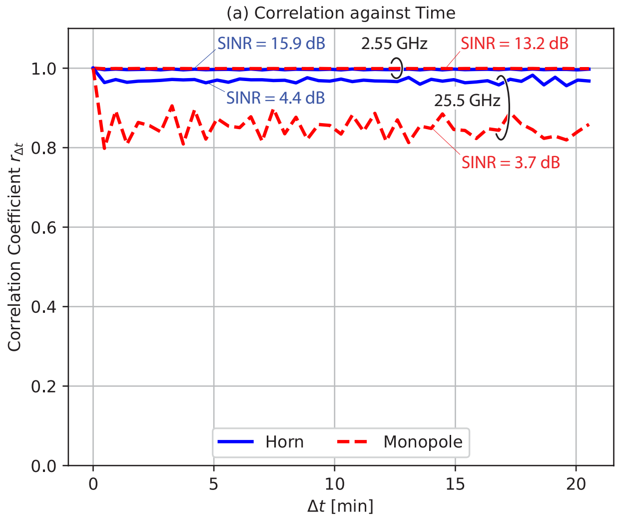

(a) The correlation between CTFs measured at the same position but at different times. The lowest measured value of channel correlation is 0.8, showing the high temporal stability of the measurement testbed.

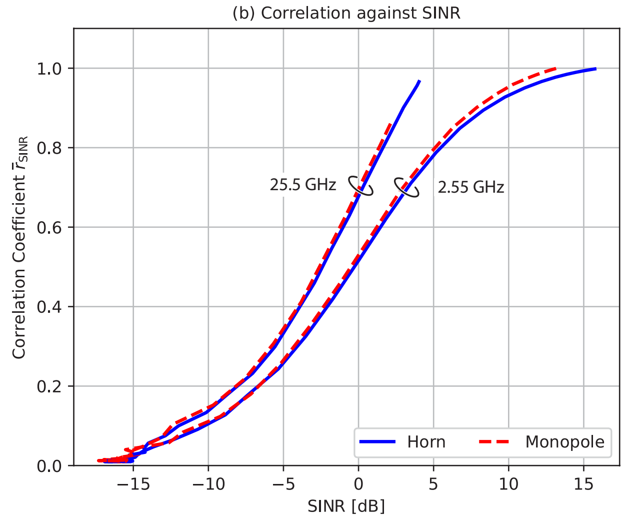

(b) The mean correlation coefficient for various SINR levels obtained by averaging against time. The mmWave scenarios exhibit larger correlation than sub-6 GHz scenarios at the same SINR level.

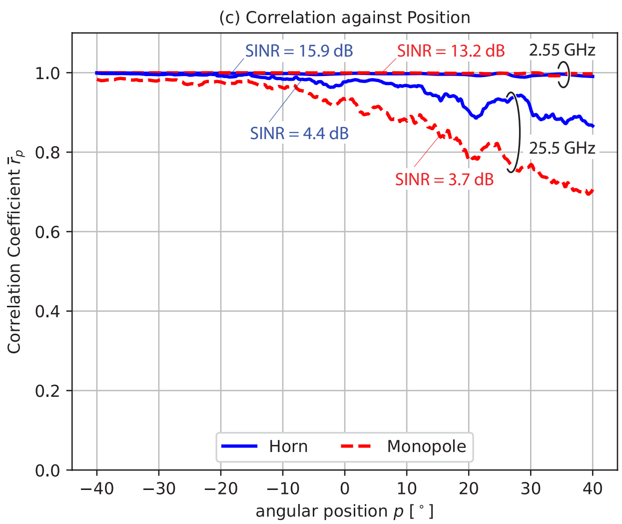

(c) The mean correlation coefficient for different angular positions obtained by averaging against time depends on the SINR and the distance from the starting point of the measurement.

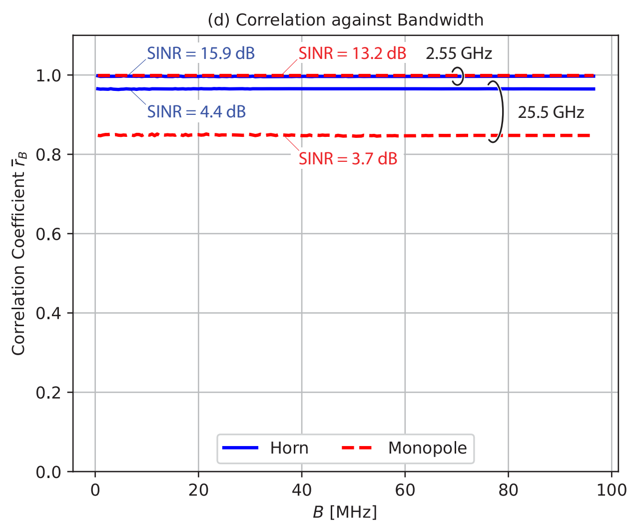

(d) The mean correlation coefficient depends mainly on the SINR and changes only marginally when different bandwidths are employed.

Fig. 4. The correlation against (a) time between measurements, (b) SINR level, (c) position within the measured trace and (d) bandwidth employed.

As expected, the correlation decreases with decreasing SINR level from its maximum value given in Tab. II to zero for all scenarios. Furthermore, for the same observed SINR level, mmWave scenarios exhibit a larger correlation coefficient than sub-6 GHz scenarios. In particular, for $\mathrm{SINR} = 0\,\mathrm{dB}$, the correlation coefficient for mmWave scenarios is approximately 0.7, while for sub-6 GHz it is about 0.5. This phenomenon occurs due to larger interference plus noise power $\overline{P}_{\mathrm{IN}}$ for sub-6 GHz bands compared to mmWave bands (see Tab. II). Employing monopole instead of horn receive antenna leads to a slightly increased correlation coefficient for both frequency bands.

D. *Correlation against Position*

Further, we analyze the temporal correlation of the channel at different angular positions of the transmit antenna at the rotary unit. In this way, we test the accuracy of the self-built trigger unit [26] employed for time synchronization as well as the phase stability of the measurement setup. As correlation metric, we employ the vector inner product given by

$$\overline{r}_n = \frac{1}{T}\sum_{\Delta t=0}^{T-1} \frac{|\mathbf{h}_{t,n}^{\mathrm{H}}\mathbf{h}_{t+\Delta t,n}|}{\|\mathbf{h}_{t,n}\|_2\|\mathbf{h}_{t+\Delta t,n}\|_2}, \tag{4}$$

where $\mathbf{h}_{t,n} \in \mathbb{C}^{K\times 1}$ denotes the CTF at discrete-time snapshot n and at measurement run t. Note that each snapshot

$n \in \{1, \ldots, N\}$ corresponds to an appropriate angular position $p \in \{-40°, \ldots, 40°\}$ within the rotary arm movement. This examines how "similar" the measured channel at a specific angular position (snapshot) is between temporally separated transmissions. In Fig. 4c, the correlation coefficient $\overline{r}_p$ is plotted against the position p of the measured trace. Note that the measured trace from $-40°$ to $40°$ with the arm length of 1 m corresponds to the trace length of 1.39 m.

One can observe that the correlation against angular position depends on the SINR and the distance from the starting point of the measurement. Due to the larger SINR, sub-6 GHz scenarios show significantly better correlation against angular positions than mmWave scenarios. Consequently, the variations of the correlation coefficient in sub-6 GHz scenarios are minor. Furthermore, the correlation coefficient decreases with increasing distance from the starting point of the measurement at $-40°$. Such a correlation decrease across angular positions occurs possibly due to the phase instability of the rotary joints employed, which is particularly obvious at low SINR. Therefore, choosing a smaller trace length would lead to an increased similarity between consecutive measurements.

E. Correlation against Bandwidth

The interference level at the receiver can be influenced by the employed signal bandwidth. As our measurement setup operates in 5G NR frequency bands n7 and n258 [27], a larger signal bandwidth increases the probability that an interferer could affect the reproducibility of the measurement results. Therefore, we investigate how different signal bandwidths affect reproducibility.

Within the total measured bandwidth of $B_{\mathrm{t}} = 100\,\mathrm{MHz}$, we select a portion b_i of the bandwidth B and average correlation coefficient over measurement runs

$$\overline{r}_B = \frac{1}{RT} \sum_{b_i=1}^{R} \sum_{\Delta t=0}^{T-1} \frac{\left|\mathrm{tr}\left(\mathbf{H}_{t,b_i}^{\mathrm{H}} \mathbf{H}_{t+\Delta t, b_i}\right)\right|}{\|\mathbf{H}_{t,b_i}\|_F \|\mathbf{H}_{t+\Delta t,b_i}\|_F}. \tag{5}$$

The bandwidth $b_i = \begin{bmatrix} k_i & \cdots & k_i + \frac{B}{\Delta f} \end{bmatrix}$ corresponds to the subcarrier k_i which is randomly chosen from the set $\{-K/2, \ldots, K/2 - 1\}$. Since the received signal power is not constant within the total bandwidth of B_{t}, the process of random selection is repeated $R = 100$ times and the obtained correlation coefficient is averaged. Averaging is performed to avoid the selected portion of the bandwidth being in a frequency selective fading hole. In this way, we examine how "similar" is the same portion of the bandwidth B between temporally separated transmissions. In Fig. 4d, the correlation $\overline{r}_B$ is plotted against the employed bandwidth B.

As in Fig. 4a, the correlation coefficient $\overline{r}_B$ depends mainly on the measured SINR level. Furthermore, in both sub-6 GHz and mmWave scenarios, one can notice that the correlation coefficient changes only marginally when different bandwidths are employed.

V. Conclusion

We conducted a measurement campaign to verify the reproducibility of the proposed testbed. We analyzed the measurement results in terms of correlation against (a) time, (b) SINR, (c) position within the measured trace and (d) bandwidth employed. The reproducibility depends strongly on the measured SINR level and only marginally on the angular trace length and the employed signal bandwidth. By ensuring a sufficiently high SINR level, the proposed testbed is able to reproduce an experiment with minor uncertainties. Using this setup, the effects of different scatterers (e.g., metallic sheets, metallic objects) introduced into the controlled environment can be accurately analyzed for both frequency bands.

Acknowledgment

This work was supported by the Austrian Research Promotion Agency (FFG) via the research project Intelligent Intersection (ICT of the Future, Grant 880830) and the Christian Doppler Laboratory for Dependable Wireless Connectivity for the Society in Motion. The work of M. Hofer and T. Zemen was supported by the principal scientist grant DEDICATE.

References

[1] M. Giordani, A. Zanella, and M. Zorzi, "Millimeter wave communication in vehicular networks: Challenges and opportunities," in *2017 6th International Conference on Modern Circuits and Systems Technologies (MOCAST)*, 2017.

[2] A. L. Gratzer, A. Schirrer, E. Thonhofer, F. Pasic, S. Jakubek, and C. F. Mecklenbräuker, "Short-Term Collision Estimation by Stochastic Predictions in Multi-Agent Intersection Traffic," in *Proc. of the International Conference on Electrical, Computer and Energy Technologies (ICECET 2022)*, 2022.

[3] B. Ai, A. F. Molisch, M. Rupp, and Z. D. Zhong, "5G key technologies for smart railways," *Proceedings of the IEEE*, vol. 108, no. 6, 2020.

[4] V. Shivaldova, A. Paier, D. Smely, and C. F. Mecklenbräuker, "On Roadside Unit Antenna Measurements for Vehicle-to-Infrastructure Communications," in *2012 IEEE 23rd International Symposium on Personal, Indoor and Mobile Radio Communications - (PIMRC)*, 2012, pp. 1295–1299.

[5] F. Pasic, S. Pratschner, R. Langwieser, and C. F. Mecklenbräuker, "High-Mobility Wireless Channel Measurements at 5.9 GHz in an Urban Environment," in *2022 International Balkan Conference on Communications and Networking (BalkanCom)*, 2022, pp. 100–104.

[6] M. Lerch, "Experimental comparison of fast-fading channel interpolation methods for the LTE uplink," in *2015 57th International Symposium ELMAR (ELMAR)*, 2015, pp. 5–8.

[7] D. Schützenhöfer, E. Zöchmann, M. Lerch, S. Pratschner, H. Groll, S. Caban, and M. Rupp, "Experimental evaluation of the influence of fast movement on virtual antenna arrays," in *WSA 2019; 23rd International ITG Workshop on Smart Antennas*, 2019.

[8] J. Kunisch and J. Pamp, "Wideband Car-to-Car Radio Channel Measurements and Model at 5.9 GHz," in *2008 IEEE 68th Vehicular Technology Conference*, 2008.

[9] Z. Su, L. Liu, Y. Fan, S. Dong, L. Zhang, J. Qiu, and X. Lin, "Measurements and Characteristics for Vehicle to Everything Channel in Tunnel Scenario at 5.9 GHz," in *2021 7th International Conference on Computer and Communications (ICCC)*, 2021, pp. 230–234.

[10] H. Fernández, V. M. Rodrigo-Peñarrocha, L. Rubio, and J. Reig, "Path Loss Characterization in Vehicular Environments under LOS and NLOS Conditions at 5.9 GHz," in *The 8th European Conference on Antennas and Propagation (EuCAP 2014)*, 2014, pp. 3044–3048.

[11] F. Kaltenberger, A. Byiringiro, G. Arvanitakis, R. Ghaddab, D. Nussbaum, R. Knopp, M. Bernineau, Y. Cocheril, H. Philippe, and E. Simon, "Broadband wireless channel measurements for high speed trains," in *2015 IEEE International conference on communications (ICC).*

[12] F. Pasic, S. Pratschner, M. Rupp, and C. F. Mecklenbräukcr, “Pilot-Aided Channel Estimation Scheme for NR- V2X Speed Emulation Technique,” in *2022 56th Asilomar Conference on Signals, Systems, and Computers*, 2022, pp. 1202–1207.

[13] A. Paier, J. Karedal, N. Czink, H. Hofstetter, C. Dumard, T. Zemen, F. Tufvesson, A. F. Molisch, and C. F. Mecklenbräuker, “Car-to-car radio channel measurements at 5 GHz: Pathloss, power-delay profile, and delay-Doppler spectrum,” in *2007 4th International Symposium on Wireless Communication Systems*, 2007, pp. 224–228.

[14] E. Zöchmann, M. Hofer, M. Lerch, S. Pratschner, L. Bernadó, J. Blumenstein, S. Caban, S. Sangodoyin, H. Groll, T. Zemen, A. Prokeš, M. Rupp, A. F. Molisch, and C. F. Mecklenbräuker, “Position-specific statistics of 60 GHz vehicular channels during overtaking,” *IEEE Access*, vol. 7, pp. 14 216–14 232, 2019.

[15] E. Zöchmann, C. F. Mecklenbräuker, M. Lerch, S. Pratschner, M. Hofer, D. Löschenbrand, J. Blumenstein, S. Sangodoyin, G. Artner, S. Caban, T. Zemen, A. Prokeš, M. Rupp, and A. F. Molisch, “Measured delay and Doppler profiles of overtaking vehicles at 60 GHz,” in *12th European Conference on Antennas and Propagation (EuCAP 2018)*, 2018.

[16] H. Groll, E. Zöchmann, S. Pratschner, M. Lerch, D. Schützenhöfer, M. Hofer, J. Blumenstein, S. Sangodoyin, T. Zemen, A. Prokeš, A. F. Molisch, and S. Caban, “Sparsity in the Delay-Doppler Domain for Measured 60 GHz Vehicle-to-Infrastructure Communication Channels,” in *2019 IEEE International Conference on Communications Workshops (ICC Workshops)*, 2019.

[17] J. Blumenstein, A. Prokes, J. Vychodil, T. Mikulasek, J. Milos, E. Zöchmann, H. Groll, C. F. Mecklenbräuker, M. Hofer, D. Löschenbrand, L. Bernadó, T. Zemen, S. Sangodoyin, and A. Molisch, “Measured high-resolution power-delay profiles of non-stationary vehicular millimeter wave channels,” in *2018 IEEE 29th Annual International Symposium on Personal, Indoor and Mobile Radio Communications (PIMRC)*, 2018.

[18] J. Park, J. Lee, K. Kim, and M. Kim, “28-GHz High-Speed Train Measurements and Propagation Characteristics Analysis,” in *2020 14th European Conference on Antennas and Propagation (EuCAP)*, 2020.

[19] D. He, B. Ai, K. Guan, Z. Zhong, B. Hui, J. Kim, H. Chung, and I. Kim, “Channel Measurement, Simulation, and Analysis for High-Speed Railway Communications in 5G Millimeter-Wave Band,” *IEEE Transactions on Intelligent Transportation Systems*, vol. 19, no. 10, pp. 3144–3158, 2018.

[20] D. Radovic, H. Groll, and C. F. Mecklenbräuker, “Evaluation of stationarity regions in measured non-WSSUS 60 GHz mmWave V2V channels,” in *2022 56th Asilomar Conference on Signals, Systems, and Computers*, 2022, pp. 1212–1216.

[21] D. Dupleich, R. Müller, M. Landmann, E.-A. Shinwasusin, K. Saito, J.-I. Takada, J. Luo, R. Thomä, and G. Del Galdo, “Multi-band propagation and radio channel characterization in street canyon scenarios for 5G and beyond,” *IEEE Access*, vol. 7, pp. 160 385–160 396, 2019.

[22] M. Hofer, D. Löschenbrand, J. Blumenstein, H. Groll, S. Zelenbaba, B. Rainer, L. Bernadó, J. Vychodil, T. Mikulasek, E. Zöchmann, S. Sangodoyin, H. Hammoud, B. Schrenk, R. Langwieser, S. Pratschner, A. Prokes, A. F. Molisch, C. F. Mecklenbräuker, and T. Zemen, “Wireless Vehicular Multiband Measurements in Centimeterwave and Millimeterwave Bands,” in *2021 IEEE 32nd Annual International Symposium on Personal, Indoor and Mobile Radio Communications (PIMRC)*, 2021, pp. 836–841.

[23] M. Hofer, D. Löschenbrand, S. Zelenbaba, A. Dakić, B. Rainer, and T. Zemen, “Wireless 3 GHz and 30 GHz Vehicle-to-Vehicle Measurements in an Urban Street Scenario,” in *2022 IEEE 96th Vehicular Technology Conference (VTC2022-Fall)*, 2022.

[24] D. Radovic, F. Pasic, M. Hofer, H. Groll, C. F. Mecklenbräucker, and T. Zemen, “Stationarity Evaluation of High-mobility sub-6 GHz and mmWave non-WSSUS Channels,” *arXiv preprint arXiv:2304.00870*, 2023.

[25] F. Pasic, M. Hofer, M. Mussbah, H. Groll, T. Zemen, S. Schwarz, and C. F. Mecklenbräucker, “Statistical Evaluation of Delay and Doppler Spreads in sub-6 GHz and mmWave Vehicular Channels,” in *2023 IEEE 97th Vehicular Technology Conference (VTC2023-Spring)*, (in press). [Online]. Available: https://owncloud.tuwien.ac.at/index.php/s/xYl86Lu6KOR92O5

[26] F. Pasic, S. Pratschner, R. Langwieser, D. Schützenhöfer, E. Jirousek, H. Groll, S. Caban, and M. Rupp, “Sub 6 GHz versus mmWave Measurements in a Controlled High-Mobility Environment,” in *WSA 2021; 25th International ITG Workshop on Smart Antennas*, 2021.

[27] 3GPP, “NR; User Equipment (UE) radio transmission and reception; Part 1: Range 1 Standalone (Release 15),” 3rd Generation Partnership Project (3GPP), Technical Specification (TS) 38.101, 2023, version 15.10.0.

[28] A. D. McNaught, A. Wilkinson *et al.*, “Compendium of Chemical Terminology. IUPAC recommendations,” 1997.

[29] F. Pasic, D. Schützenhöfer, E. Jirousek, R. Langwieser, H. Groll, S. Pratschner, S. Caban, S. Schwarz, and M. Rupp, “Comparison of Sub 6 GHz and mmWave Wireless Channel Measurements at High Speeds,” in *16th European Conference on Antennas and Propagation (EuCAP 2022)*, 2022.

[30] S. Caban, J. Rodas, and J. A. García-Naya, “A methodology for repeatable, off-line, closed-loop wireless communication system measurements at very high velocities of up to 560 km/h,” in *2011 IEEE International Instrumentation and Measurement Technology Conference*, 2011.

[31] B.-J. Choi, E.-L. Kuan, and L. Hanzo, “Crest-factor study of MC-CDMA and OFDM,” in *50th Vehicular Technology Conference*, vol. 1, 1999.